*M. Kuna*, H. Kordisch†, and A. Ockewitz†*

# Thermoelastic–Plastic FEM-Analysis of a Semi-Elliptical Surface Crack in a Cylinder under Non-Axi-Symmetric Cooling

**REFERENCE** Kuna, M., Kordisch, H., and Ockewitz, A., **Thermoelastic–plastic FEM-analysis of a semi-elliptical surface crack in a cylinder under non-axi-symmetric cooling,** *Defect Assessment in Components – Fundamentals and Applications*, ESIS/EGF9 (Edited by J. G. Blauel and K.-H. Schwalbe) 1991, Mechanical Engineering Publications, London, pp. 101–115.

**ABSTRACT** A cylindrical model of a pressure vessel with an inner surface crack is analysed under a defined pressurized thermal shock scenario. Here, a periodical formation of coolant strips is assumed along the perimeter of the cooled inner vessel surface. Semi-elliptical surface cracks (ASME-d/4-flaw) are consisdered in circumferential orientation at the centre of the coolant strips, which experience maximum tensile loading during this type of cooling. Using finite elements, the three-dimensional transient temperature fields and the corresponding combined thermomechanical stresses in the cylinder with flaw are analysed for temperature-dependent elastic–plastic material behaviour of the base metal and the cladding. Emphasis is layed on the nonlinear fracture behaviour by investigating $J$-integral and crack opening displacements. Consequences for the integrity of the component can be deduced from the assessment of the safety margins against fracture.

## Introduction

During a loss of coolant accident in nuclear pressurized water reactors the pressure vessel is exposed to both sudden cooldown temperatures and simultaneous high pressure loading (pressurized thermal shock PTS), which causes strong temperature gradients and stresses ranging far above the usual in-service loads. Because of the reduced temperature and the intensive neutron embrittlement, the fracture toughness of the material is particularly decreased at the inner side of the wall so that the safety against crack initiation has to be assessed. Up to now mainly cracks in axial orientation have been investigated, which are maximum loaded for homogeneous cooling conditions along the circumference of the cylinder. Recent investigations **(1)**, however, show that the highest stresses acting on circumferentially orientated cracks occur under a strip-like formation of the cooling medium. An elastic–plastic fracture assessment may be particularly important for the circumferential weld located above the active core zone, since here the lowest embrittlement but the highest thermomechanical loading is found.

* Institute of Solid State Physics and Electron Microscopy, Academy of Sciences of the GDR, 4020 Halle, GDR.
† Fraunhofer Institute of Werkstoffmechanik, 7800 Freiburg, FRG.

## The computational model

*Geometry*

The vessel considered has the following dimensions (in mm):

| | |
|---|---|
| outer radius | $r_a = 1920$ |
| inner radius (base material) | $r_{ig} = 1780$ |
| inner radius (cladding) | $r_{ip} = 1771$ |
| thickness of cladding | $= 9$ |
| wall thickness (without cladding) | $d = 140$ |

The injection of the coolant proceeds simultaneously at periodical distances of 60 degrees along the circumference of the cylinder. The coolant streams in about 30 degrees wide strips – the so-called cold zone – alternating with a warmer zone (see Fig. 1). A semi-elliptical surface crack is assumed at the inner side of the cylinder in the centre of each cold zone, since there the maximum tensile stresses are to be expected during the PTS. Due to symmetry only one half of the six equal segments needs to be modelled. Thus the FEM-discretization is restricted to the dashed region (30 degrees) of Figs 1 and 2. In order to reduce the computational effort, an artificial symmetry is introduced in axial $x$-direction with respect to the crack plane concerning geometry and loading. This approximation is considered to be conservative. Below the cooled region extending over 2700 mm, one part of length $l_a$ is appended to the cylinder allowing a free relaxation of the thermal stresses.

$l_a = 1300 \text{ mm} > 2.5(dr_i)^{1/2}$.

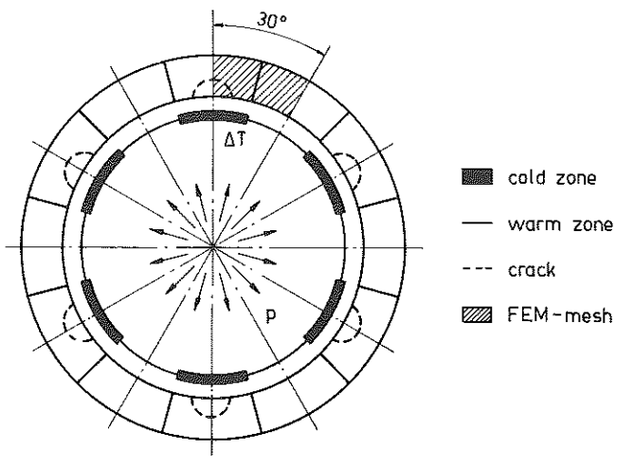


Cylinder with semi-elliptical surface crack under strip-shaped cooling

30°-model for periodical configuration along the circumference.

**Fig 1 Schematic drawing of the coolant strips formed along the circumference of the cylinder**



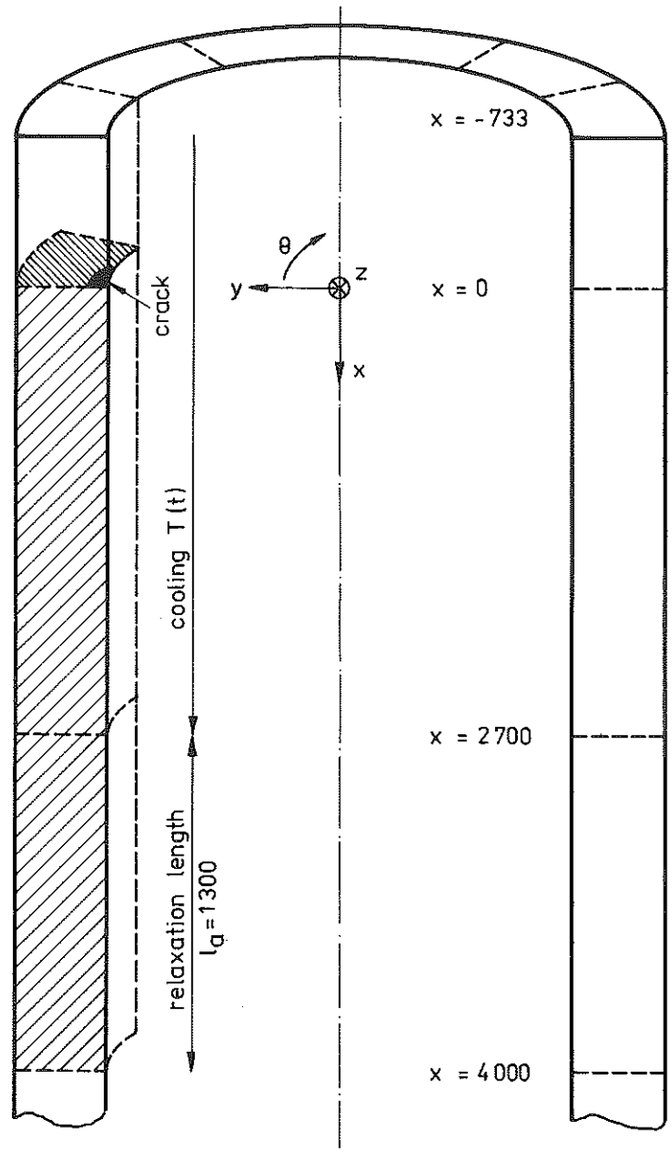


Computational model of a cylinder with semi-elliptical surface crack under strip-shaped cooling

**Fig 2 View of the computational model in axial direction of the cylinder**

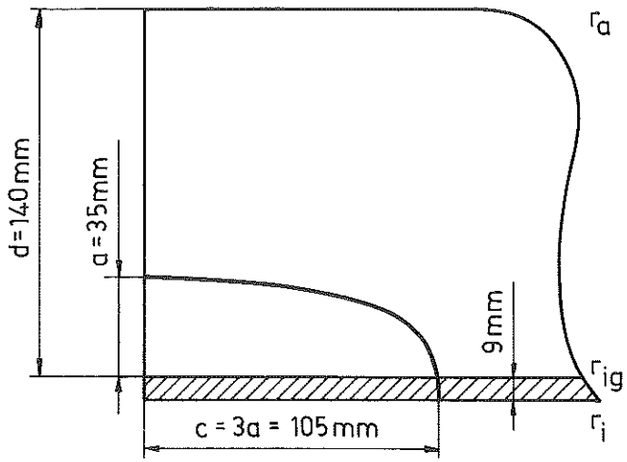


**Fig 3 ASME-d/4-surface crack in the cladded cylinder wall**

The crack was chosen according to the ASME-code recommendations ($a = d/4$, $a/c = 1/3$), disregarding the cladding, see Fig. 3.

*Pressurized thermoshock loading*

Figure 4 shows the temporal behaviour of the coolant temperatures in the cold zone and the warm zone for the considered long-term PTS scenario. Furthermore, the variation of the pressure $p$ is included. The slow decline of temperature in the warm zone is due to the average reduction of the coolant temperature in the whole primary loop. No variations of temperature, width or heat transfer of the cold zone along its height were taken into consideration, which would relieve the thermal shock in any way.

The vessel consists of a ferritic base material with austenitic cladding. For the heat conduction problem all material data are taken to be independent of temperature. They are given in Table 1 for an average temperature. The heat transfer coefficient of $h = 0.00348$ W/mm$^2$ K was chosen for the cold zone, and of $h = 0.00116$ W/mm$^2$ K for the warm zone. The thermoelastic–plastic

**Table 1 Heat conduction coefficient $\lambda$ and specific heat $c$ at 170°C**

| | $\lambda$ (W/mmK) | $c$ (J/mm$^3$K) |
|---|---|---|
| base material | 0.03789 | 0.004235 |
| cladding | 0.0186 | 0.003833 |



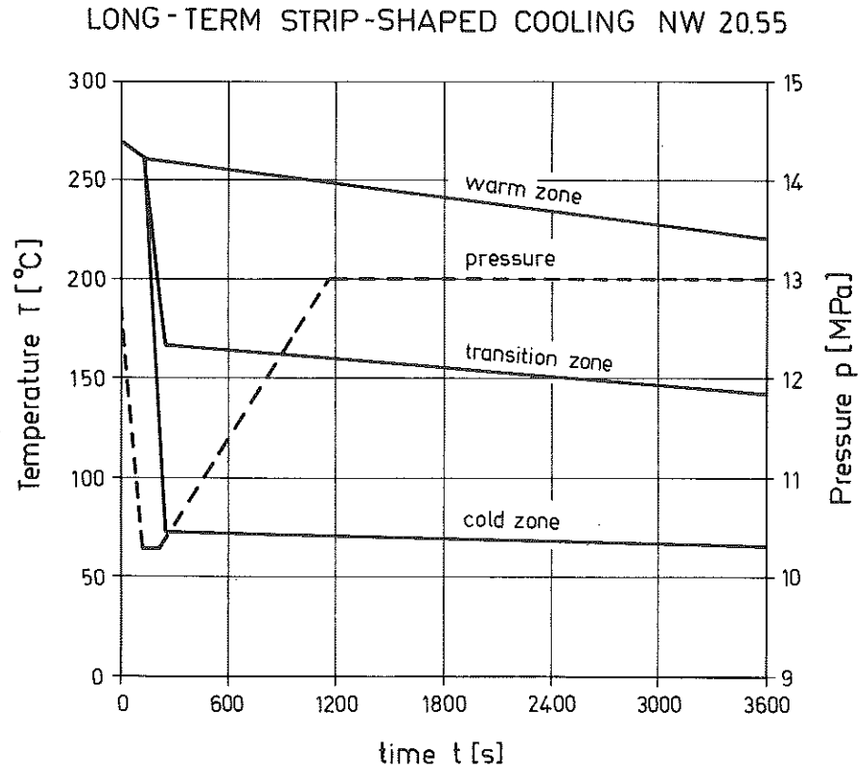


**Fig 4 Temporal behaviour of the coolant temperatures inside and outside the cooling strips and of the pressure in the course of the considered PTS**

**Table 2 Thermoelastic–plastic material constants**

| *Temperature (°C)* | *20* | *100* | *200* | *300* |
|---|---|---|---|---|
| | *Base material* | | | |
| $E$-modulus (N/mm$^2$) | 209 000 | 207 000 | 204 000 | 187 000 |
| Yield stress (N/mm$^2$) | 382 | 372 | 352 | 342 |
| Hardening mod. (N/mm$^2$) | 625 | 625 | 625 | 625 |
| Poisson's ratio | 0.3 | 0.3 | 0.3 | 0.3 |
| Heat expansion coefficient (1/K) | 10.9E-6 | 10.9E-6 | 11.5E-6 | 12.3E-6 |
| | *Cladding material* | | | |
| $E$-modulus (N/mm$^2$) | 190 000 | 190 000 | 190 000 | 190 000 |
| Yield stress (N/mm$^2$) | 775 | 720 | 651 | 582 |
| Hardening mod. (N/mm$^2$) | 2210 | 1879 | 1465 | 1051 |
| Poisson's ratio | 0.3 | 0.3 | 0.3 | 0.3 |
| Heat expansion coefficient (1/K) | 16.6E-6 | 17.0E-6 | 17.2E-6 | 17.5E-6 |

material behaviour was treated as isotropic, linear hardening, and temperature-dependent. The values used for both materials are summarized in Table 2 as a function of temperature.

### Analysis of the transient heat conduction problem

To determine the temperature distribution in the cylinder during the thermal shock process, the transient heat conduction problem was solved utilizing the FEM-System ADINAT (2). Figure 5 depicts the FEM-mesh ZYL3 used for the 30 degree segment. For convenience, the modelling of the crack was omitted, as it does not influence the heat conduction. The first element sheet represents the cladding. Along the inner perimeter six elements are used for both the cold and warm zones. The following boundary conditions are specified for the different regions of the model (see also Fig. 2):

symmetry plane ($\theta = 0$): zero heat flux
plane of periodicity ($\theta = 30$ degrees): zero heat flux
top face ($x = 0$): zero heat flux
bottom face ($x = 4000$): isolation
outer surface ($r = r_a$): isolation
inner surface (relaxation part): ($2700 < x < 4000$, $r = r_i$): isolation
inner surface (cooling region) ($0 < x < 2700$, $r = r_i$):
linear heat transfer with different environmental temperatures and heat transfer coefficients for the cold zone ($0 < \theta < 15$ degrees) and for the warm zone ($15 < \theta < 30$ degrees) see Fig. 4 and Table 1. At the border line between both zones a mean value of the environmental temperature was applied (see Fig. 4) to avoid numerical oscillations.

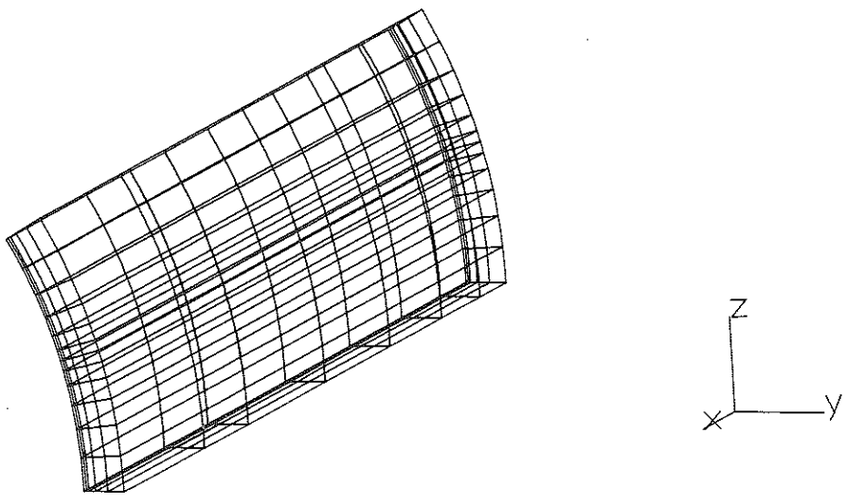


**Fig 5 Finite element mesh ZYL3 for the analysis of the transient heat conduction in the cylinder (30 degree-model, 420 elements, 2266 nodes)**



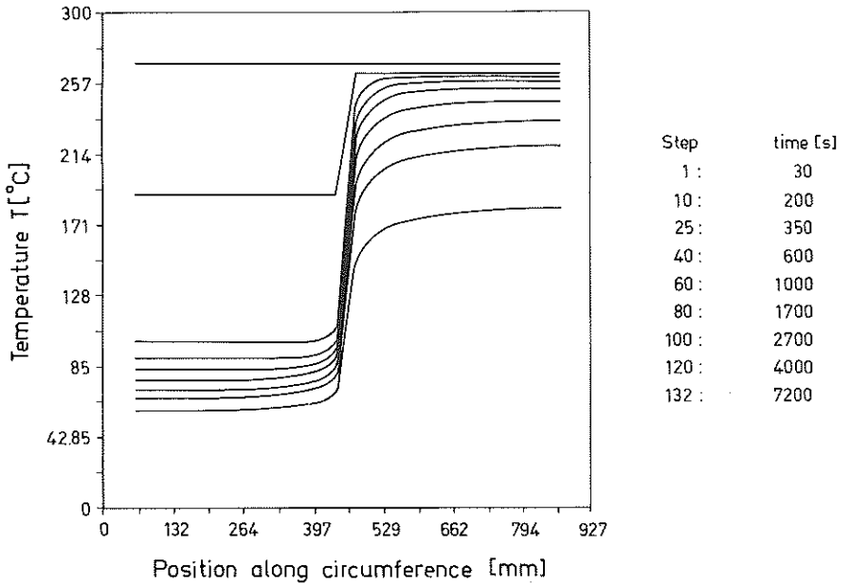


**Fig 6 Computed temperature distribution as function of time at the inner surface of the cylinder**

A total number of 136 time steps (5 × 30 s, 25 × 10 s, 40 × 20 s, 48 × 50 s, 18 × 200 s) was prescribed, covering a period of 7200 seconds counted from the beginning of the thermal shock.

The time-dependent temperature distributions along the perimeter at the inner surface at $x = 0$ and $0 < \theta < 30$ degrees (prospective crack plane) are illustrated in Fig. 6. The different temperatures formed at the cold and warm

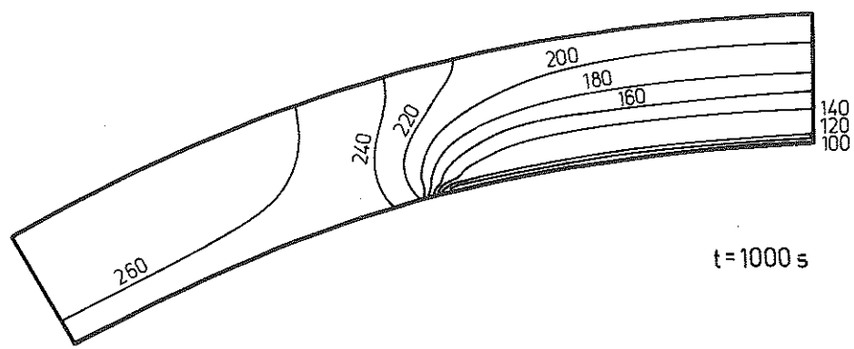


Temperature distribution in the crack plane

**Fig 7 Isolines of temperatures on the crack plane at 1000 s**

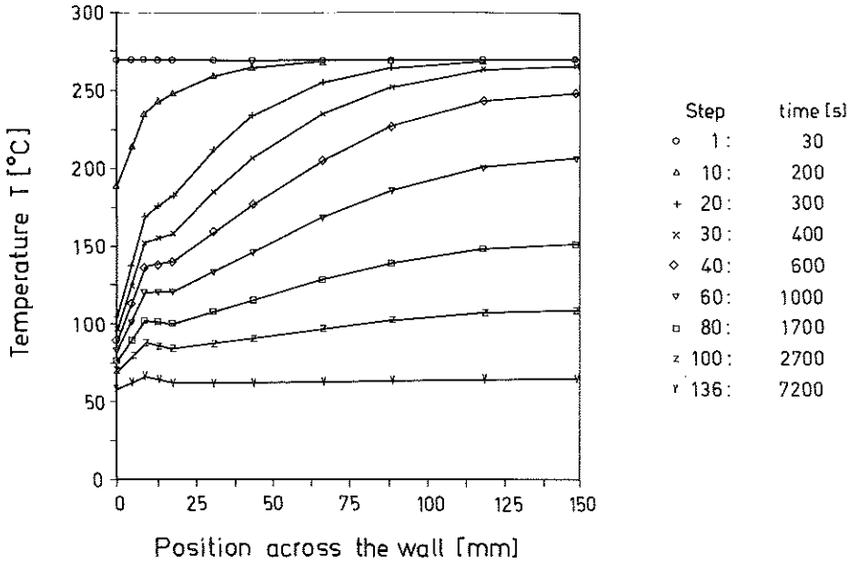


**Fig 8 Transient temperature field across the cylinder wall in the centre of the cold zone**

zones can clearly be distinguished, connected by a steep transition region. A full view of the temperatures in the crack (top) plane is given in Fig. 7. The transient temperature field across the wall thickness is shown in Fig. 8 for the centre of the cold zone ($\theta = 0$).

## Analysis of the thermoelastic–plastic crack problem

### *The computational model*

The stress analysis of the cylinder with a crack under pressurized thermal shock loading was crarried out by means of the FEM-system ADINA **(3)** using the fracture mechanical supplements of IWM CRACK **(4)**. For the considered 30 degree-segment of the cylinder (dashed in Fig. 2) the FEM-mesh RISS3 was constructed with the semi-elliptical ASME-d/4-crack being placed in the centre of the cooling strip, see Fig. 9. Each segment of the crack front is surrounded by two rings of six elements. The inner ring consists of collapsed elements with independent nodal displacements allowing a $1/r$-singularity for the strains.

The pressure $p$ acts on the whole inner surface of the 30 degree-segment. Since the vessel is closed, the pressure causes also an axial tensile stress of

$$p' = pr_i^2/(r_a^2 - r_i^2) = 5.703p,$$

which is applied to the bottom face of the FEM-model. Both $p$ and $p'$ obey the time function shown in Fig. 4. Furthermore, the following boundary conditions were applied:

| | |
|---|---|
| symmetry plane ($\theta = 0$): | normal displacement $u_z = 0$ |
| plane of periodicity ($\theta = 30$ degrees): | constraint condition $u_z = \tan(30)u_y$ |
| top face ($x = 0$): | normal displacement $u_x = 0$ |
| crack face: | pressure loading $p$ |
| outer surface ($r = r_a$): | stress free |



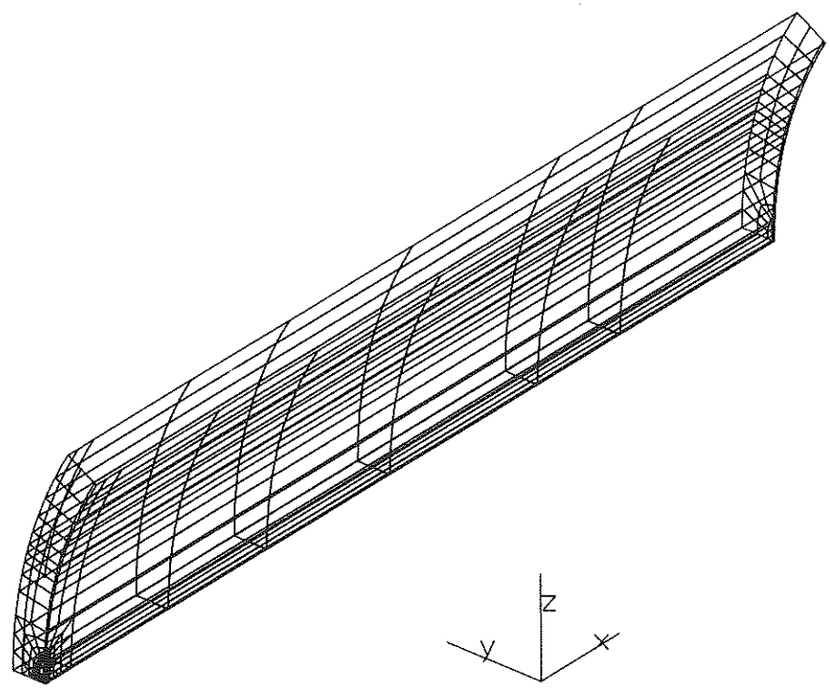


**Fig 9 FEM-mesh RISS3 for the 30 degree-model of the cylinder with semi-elliptical surface crack. 580 isoparametric 20-node brick elements, 3193 nodes**

Simultaneously with the pressure, the transient thermal loads were taken into account. For that reason the temperature fields obtained by means of the mesh ZYL3 were interpolated to the mesh RISS3 for all time intervals and used as input data for ADINA. The incremental elastic–plastic analysis was extended over 7200 s by 69 load steps of appropriate size. The service temperature of the reactor (270°C) was regarded as the reference temperature, at which the cylinder is considered to be free of stresses.

### *Results*

Despite the initial fluctuation in the system pressure (see Fig. 5), the temporal behaviour of the stresses is essentially governed by the thermal loads, which is typical for all PTS-scenarios. At first the axial stresses in the cylinder region

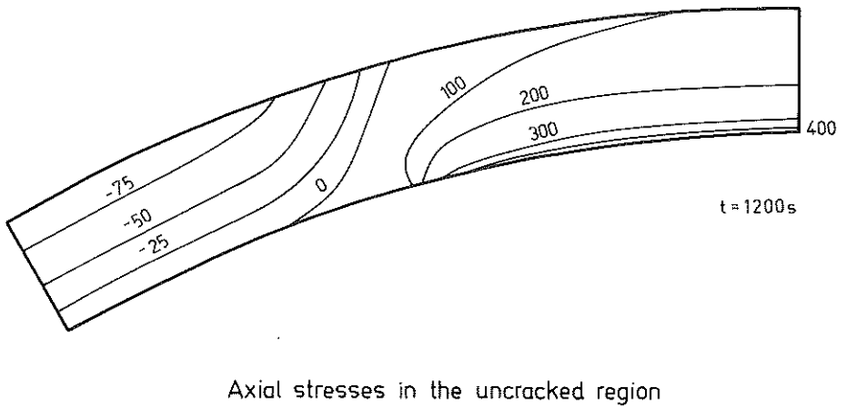


**Fig 10 Axial stresses in the cross-section of the cylinder far away from the crack after 1200 s**

far away from the crack ($x = 1215$ mm) are investigated, which should be representative of the uncracked cylinder. The results reveal that at the initial stage of the PTS there is a tension–compression state across the cylinder wall in the region of the cold zone, whereas with increasing time the whole cold zone region experiences a tension against the compressed region of the warm zone, see Fig. 10. At the end of the long-term cooling a homogeneous low temperature level will be reached producing no eigen-stresses so that only the

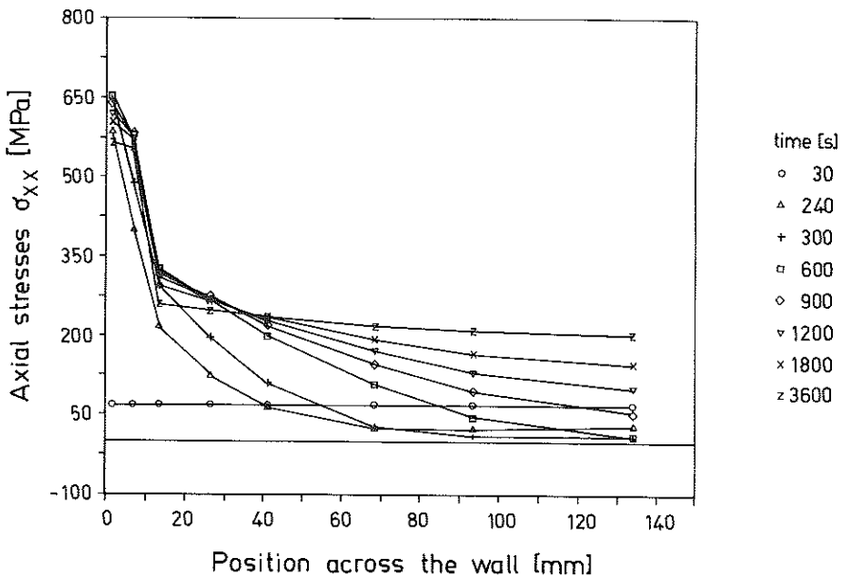


**Fig 11 Temporal variation of the axial stresses across the cylinder wall in the centre of the cold zone**



axial tension $p'$ prevails. Figure 11 illustrates the axial stresses along a radial line through the wall in the middle of the cold zone. A high stress concentration is observed at the surface, especially in the cladding, which is due to the steep temperature gradient (see Fig. 8) and the larger coefficient of thermal expansion of the austenite. Because of the plastification the stresses in the cladding do not exceed a maximum value. The plastic deformation is restricted particularly to the crack region and the cladding.

The crack opening displacements of the crack face are shown in Fig. 12 during the course of PTS-loading. The crack profile in the radial/axial cross-section is depicted. The crack opening attains its maximum after about 600–900 seconds and reduces to about 80 percent at the end of the cooling. This behaviour is in good coincidence with the peak curves of the stresses and of the $J$-integral.

Particular attention was drawn to the $J$-integral as an important parameter in elastic–plastic fracture mechanics. $J$ was calculated by means of the virtual crack extension technique **(5)**, with two paths (both the inner rings) being examined for each corner node position along the crack front. The maximum

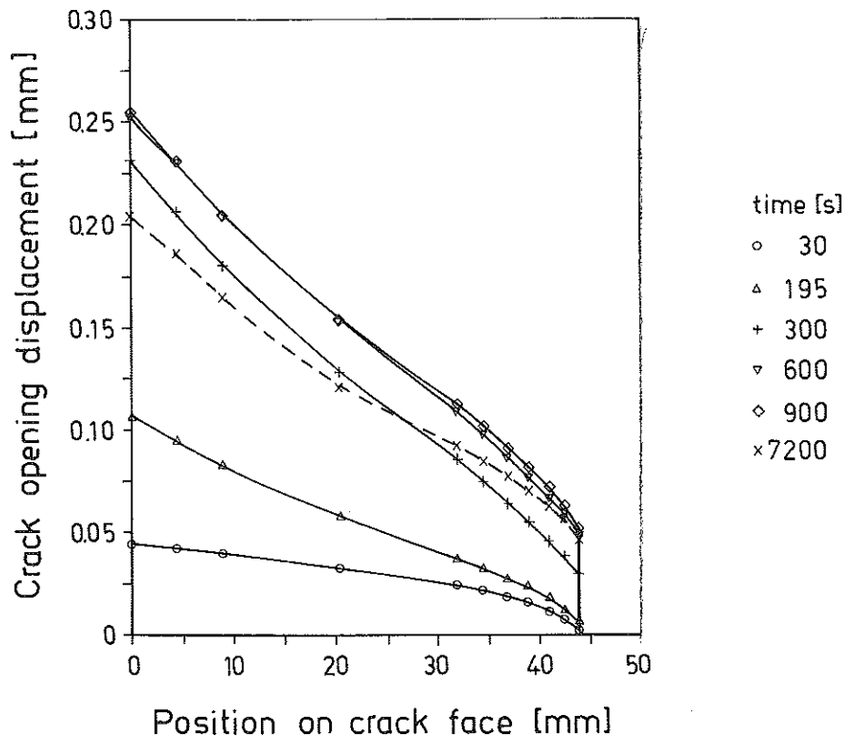


**Fig 12 Temporal behaviour of the crack profile in a radial cross-section in the centre of the cold zone**

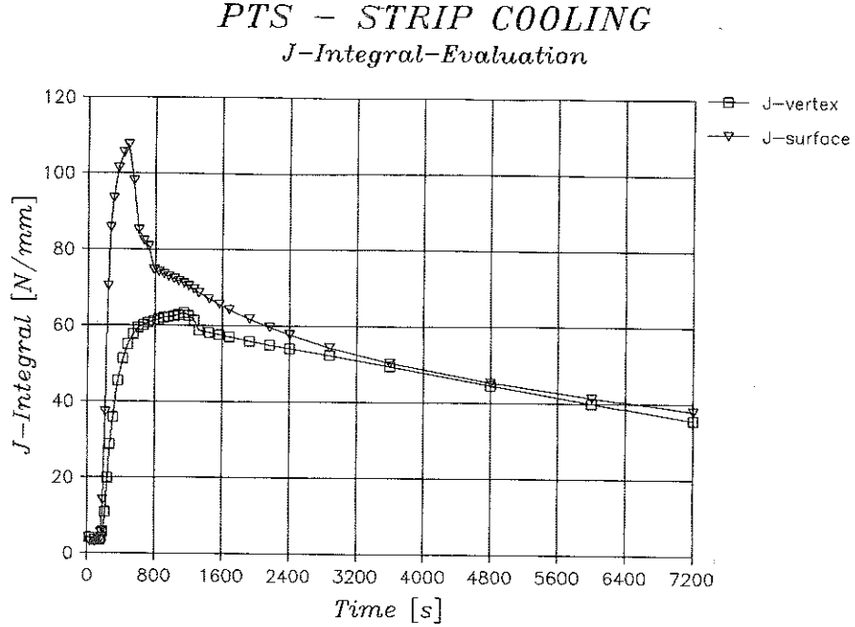


**Fig 13 Dependence of the *J*-integral on time for the deepest point of the crack and at the surface**

differences between the *J*-values computed on the two paths amounted to 10 percent. The values of the outer path are regarded as more reliable, which is why they are represented in the following. In order to verify the computation technique for *J*, the *J*-values obtained for the pure elastic pressure load of this crack configuration were compared with the $K_I$-approximation formulae implemented in the code IWM-VERB **(6)**. The FEM-results gave satisfactory agreement with the $K_I$ solutions for an equal semi-elliptical crack in a pressurized cylinder or in an uniaxial tension plate, respectively.

The temporal behaviour of *J* is shown in Fig. 13 at the vertex of the crack front and at its intersection with the cylinder surface. After a first drop, due to the initially reduced pressure, *J* rapidly increases with the onset of the thermal shock. As expected, *J* reaches its absolute maximum value of *J*-surface = 107.5 N/mm at the surface in the cladding after 480 seconds. At the deeper-lying vertex point, the maximum of *J*-vertex = 63.4 N/mm is clearly attained later, at 1140 seconds. Having passed the maxima, *J* decreases rather slowly, retaining values still around 36 N/mm after 2 h of cooling. From the distribution of *J* along the crack front, Fig. 14, one can see that *J* is strongly elevated in the cladding near the surface, whereas elsewhere a relatively constant behaviour is observed.

Discussing the stability and the growth behaviour of the crack requires a comparison to be made with the fracture toughness data. Nominal fracture



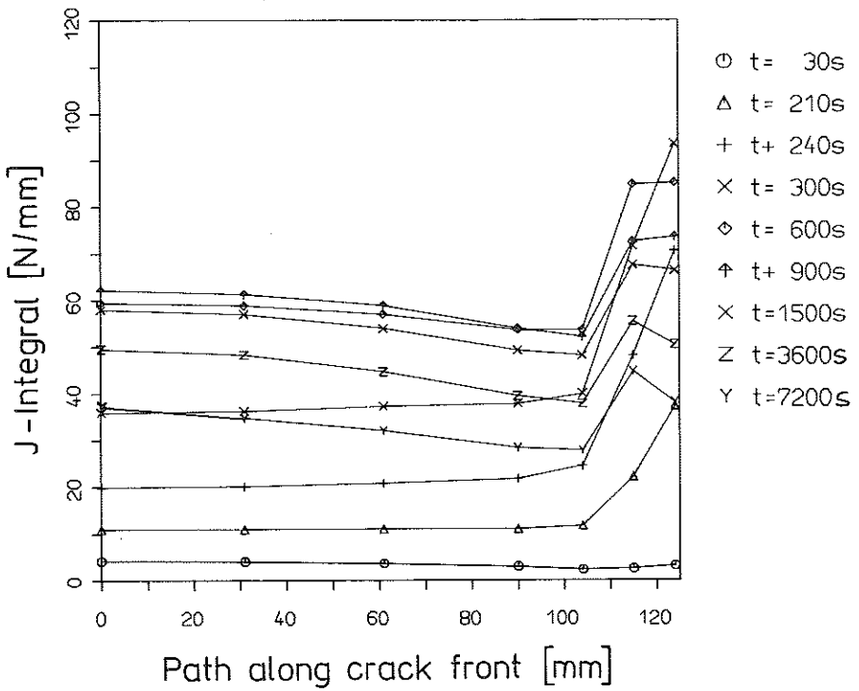


**Fig 14 Distribution of the *J*-integral along the crack front as function of time ($x = 0$ vertex, $x = 124$ surface)**

toughness curves of the weldment are given in the regulatory guideline **(7)**. As an example, the value of $T_{NDT} = 0°C$ was selected for the nil-ductile transition temperature, which may be specified for the actual situation. The computed values of *J*-vertex were converted into equivalent stress intensity values $K_I^2 = J(1 - \nu^2)/E$. These loading parameters were presented in dependence on the crack tip temperature in Fig. 15 together with the reference toughness curve $K_{IR}$. As the comparison shows, there is a considerable safety distance against crack initiation. Expressed in terms of $T_{NDT}$, it amounts to 65 degrees or about 120 degrees if the warm prestress effect is taken into account. A pure linear–elastic failure assessment may be questionable, since the above stress analysis revealed moderate plastic deformations. However, usually measured $J_{Ic}$-data of the base material far much exceed the computed *J*-values, supporting the conclusion also within the concept of ductile fracture mechanics.

## Conclusions

A cylindrical model of a reactor pressure vessel exposed to a definite pressurized thermal shock loading was analysed by means of the finite element method. In contrast to previous studies, the influence of coolant strips

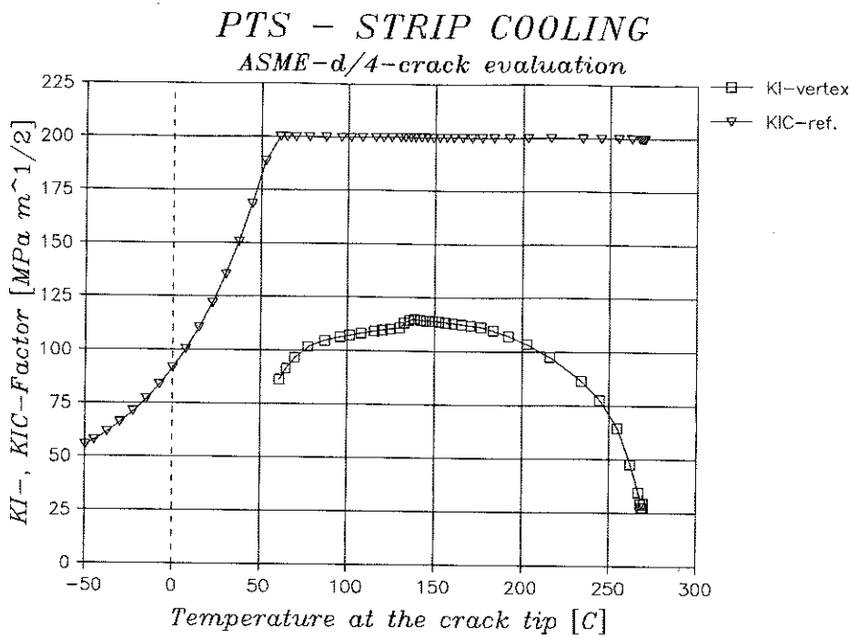


**Fig 15 Dependence of the stress intensity factor at the crack vertex on the crack tip temperature during the pressurized thermal shock and the fracture toughness reference curve**

arranged periodically along the circumference was investigated. The computations yielded the transient temperature fields, the corresponding thermomechanical stresses in the cylinder and the elastic–plastic fracture parameters ($J$-integral, COD) for a semi-elliptical inner surface crack in the centre of the coolant strip, respectively. The most important results can be summarized as follows:

- The arrangement of cooling strips leads to higher axial stresses and crack loading than an axial-symmetrical homogeneous cooling.
- During the PTS the maximum stresses occur in the centre of the cooling strip in axial direction in the cladding during the time interval between 600–900 seconds. They amount to 650 MPa.
- Even after a long time of 1–2 hours, a nearly homogeneous tensile stress of about 250 MPa remains in the cold zone across the cylinder wall.
- The stresses and fracture parameters exhibit a pronounced peak curve which is due to the dominating influence of the increasing and dropping off thermal loads. This feature is typical for realistic thermoshock scenarios, whereas a more artificial cooling system as in the HDR-experiments **(1)** leads to monotonically increasing loads.
- The $J$-integral attains its maximum value at the surface in the cladding ($J$ = 107.5 N/mm at 480 s) while its highest value at the crack vertex in the base material amounts to $J$ = 63.4 N/mm at 1140 s. This means, the loading parameters would favour a lateral extension of the crack, but the higher toughness of the cladding certainly counteracts this tendency.

The plastic deformation is mainly restricted to the crack region and the cladding. To assess the effect of plasticity, pure elastic control calculations will be done for comparison in the future.



## Acknowledgements

This research was done during a working stay of the first author at IWM Freiburg in 1988 within the framework of the Treaty on Culture and Science between GDR and FRG. The support of the directors of both institutes (IWM: Prof. E. Sommer, IFE: Prof. V. Schmidt) for this project is gratefully acknowledged.

## References

**(1)** STEGMEYER, R. *et al.* (1988) 3D-FE-Analysen an einem Druckbehälter unter Thermoschock, 14. MPA-Seminar Stuttgart.
**(2)** BATHE, K. J. (1984) ADINAT-84 – Analysis of heat transfer and field problems, *Users Manual*, ADINA Eng. Inc. Watertown, USA.
**(3)** BATHE, K. J. (1984) ADINA-84 a finite element program for automatic dynamic incremental nonlinear analysis, *Users Manual*, ADINA Eng. Inc. Watertown, USA.
**(4)** IWM-CRACK, Programmpaket für bruchmechanische Probleme, Fraunhofer-Institut für Werkstoffmechanik, Freiburg.
**(5)** de LORENZI, H. G. (1985) Energy release rate calculations by the finite element method, *Eng. Fracture Mech.*, **21**, 129–143.
**(6)** HODULAK, L. (1988) IWM – VERB, Programmdokumentation, Forschungsbericht IWM Freiburg.
**(7)** State committee for application of atomic energy of USSR (1981) Recommendation for the evaluation of brittle fracture in nuclear pressure vessels, OKB Gidropress, Moscow.